

SUPPORTING INFORMATION

Indium Oxide—Single-Walled Carbon Nanotube Composite for Ethanol Sensing at Room Temperature

James E. Ellis¹, Uri Green¹, Dan C. Sorescu^{2, 3}, Yong Zhao¹, and Alexander Star^{1}*

1. Department of Chemistry, University of Pittsburgh, Pittsburgh, Pennsylvania 15260, United States

2. United States Department of Energy, National Energy Technology Laboratory, Pittsburgh, Pennsylvania 15236, United States

3. Department of Chemical and Petroleum Engineering, University of Pittsburgh, Pittsburgh, Pennsylvania 15260, United States

*Address correspondence to astar@pitt.edu

Experimental Methods

Oxidized SWCNTs (o-SWCNTs, containing surface oxygen functional groups between 1.0 and 3.0 atomic %) were purchased from Carbon Solutions, Inc. and used as received. The growth of the In_2O_3 crystalline structure on the surface of the individual SWCNTs was achieved through a sol-gel synthesis approach, as illustrated in Figure 1 through a reaction with indium hydroxide in basic pH. The indium hydroxide solution was prepared by dispersing InCl_3 (Sigma-Aldrich, 10 mg, .005 mmol) in aqueous ammonia (1.5 mL, 28-30 wt% NH_3) solution. This solution is slowly added (over an hour) to ox-SWCNTs (P3-SWCNT, Carbon Solutions Inc., 0.5 mg) sonicated in ethanol (17 mL), and stirred for an additional hour. The solution was dialyzed in water overnight. The dialyzed solution was filtered and the solid was collected. The growth of the crystalline structure of the In_2O_3 was controlled by utilizing the furnace of a thermo-gravimetric analyzer (TGA) for the annealing process. This was achieved by monitoring the thermo-gravimetric profile of samples at constant heating and nitrogen flow rates (5 °C/min, 100 ml/min), and terminating the sequence at selected points. Transmission electron microscopy (FEI Morgagni, TEM), high-resolution TEM (JEOL JEM-2100F, HRTEM), and scanning electron microscopy images (Phillips XL30 FEG, SEM) (Figure 1,2c) illustrated the morphology of this ox-SWCNT@ In_2O_3 hybrid material. Using X-ray diffraction (Bruker D8 Discover, GADDS Detector, XRD) and UV spectroscopy^{S1} (PerkinElmer Lambda 900) the crystallinity of the resulting nanostructures generated *via* this method was further confirmed (Figure 1h, Figure S4). DRIFTS (Shimadzu IRPrestige-21, Pike Technologies Easidiff DRIFTS accessory) and XPS

(Escalab 250 XI Thermo Scientific XPS) confirmed the presence of hydroxy groups on the In_2O_3 surface (Figure S3, 5). For XPS, the sample surface was cleaned with Ar ion etching to remove any hydrocarbon contamination.

Gas sensing experiments were performed using Si chips fabricated in-house, and connected to 40 CERDIP packages with Au wires. Each Si chip contained 4 devices with interdigitated gold electrodes. In_2O_3 /SWCNT solution (1 mg/ml in DI water) was dropcasted on a single chip (3 μL , solvent was allowed to evaporate on a 120 °C hot plate), placed on a test board (bias voltage: 500 mV), and sealed in a Teflon chamber. Using a Keithley Dual SourceMeter 2602 and Keithley Switching Matrix 708A, which allows 4 data outputs simultaneously, changes in electrical conductance were collected with Zephyr data-acquisition software (<http://zephyr.sourceforge.net>). Two gas flow controllers allowed the gas environment over the chip to be manipulated. For every experiment, ten minutes of 300 sccm dry N_2 (Matheson Tri-gas) was flowed over the chip to expel the sealed Teflon chamber of O_2 . Afterwards, acetone (20 ppm in dry N_2 , Matheson Tri-gas) or ethanol (200 ppm in dry N_2 , Liquid Technology Corp.) was flowed at a given concentration for a two minute burst, and allowed to return back to baseline in dry N_2 for three minutes. This process was repeated so that six different, increasing concentrations of acetone or ethanol were flowed over the same chip for a single run.

Computational Methods

The adsorption and electronic properties of acetone and ethanol on $\text{In}_2\text{O}_3(111)$ surface and on a $(\text{In}_2\text{O}_3)_8$ /carboxyl/SWCNT hybrid system have been investigated using plane-wave density functional theory. Calculations were performed using Vienna ab initio simulation package.^{S2,S3} Plane wave basis sets were employed together with the PBE functional^{S4} and

projector augmented wave (PAW) pseudopotentials.^{S5,S6} A cutoff energy of 400 eV was used for the plane-wave basis set. Corrections for on-site Coulomb interactions using the GGA+U procedure, were done using an effective $U=7$ eV parameter for In atom which was tested previously in band structure and defect calculations.^{S7,S8,S9}

Adsorption on $\text{In}_2\text{O}_3(111)$ surface has been done using a slab model containing 8 layers for a total of 64 In and 96 O atoms. Neighbor slabs are separated by a vacuum width of 16 Å. Both the adsorbate molecules and all atoms in the upper half of the slab were allowed to relax during optimizations while the atoms in the bottom half of the slab were kept frozen at bulk optimized positions. The Brillouin zone was sampled with a 3x3x1 Monkhorst-Pack^{S10} grid of k-points. The adsorption energy of the adsorbate molecule was determined using the equation $E_{\text{ads}}=(E_{(\text{A})}+E_{(\text{S})}-E_{(\text{A+S})})$ where $E_{(\text{A})}$ is the energy of the isolated adsorbate A, $E_{(\text{S})}$ is the total energy of the relaxed slab, and $E_{(\text{A+S})}$ is the energy of the combined adsorbate-slab system in the optimized configuration. Stable adsorption configurations correspond in this sign convention to positive adsorption energies.

In the case of the hybrid indium oxide/carboxyl/SWCNT we used a (14,0) SWCNT with four repeating units along the tube axis leading to a system with 224 carbon atoms. Due to the large size of the supercell model used in this case with dimension $21 \times 17.04 \times 44$ Å³ sampling has been done using the Γ point during optimization while a 1x9x1 K-point grid was used in density of states calculations. The initial structure of the $(\text{In}_2\text{O}_3)_8$ nanocluster adsorbed on SWCNT was that determined previously by Walsh and Woodley^{S11} based on an evolutionary computational approach. The charge transfer between adsorbate molecules and the indium oxide surface or between the oxide nanoparticle and the SWCNT was analyzed using Bader charges^{S12} determined using the charge density decomposition method of Henkelman *et al.*^{S13}

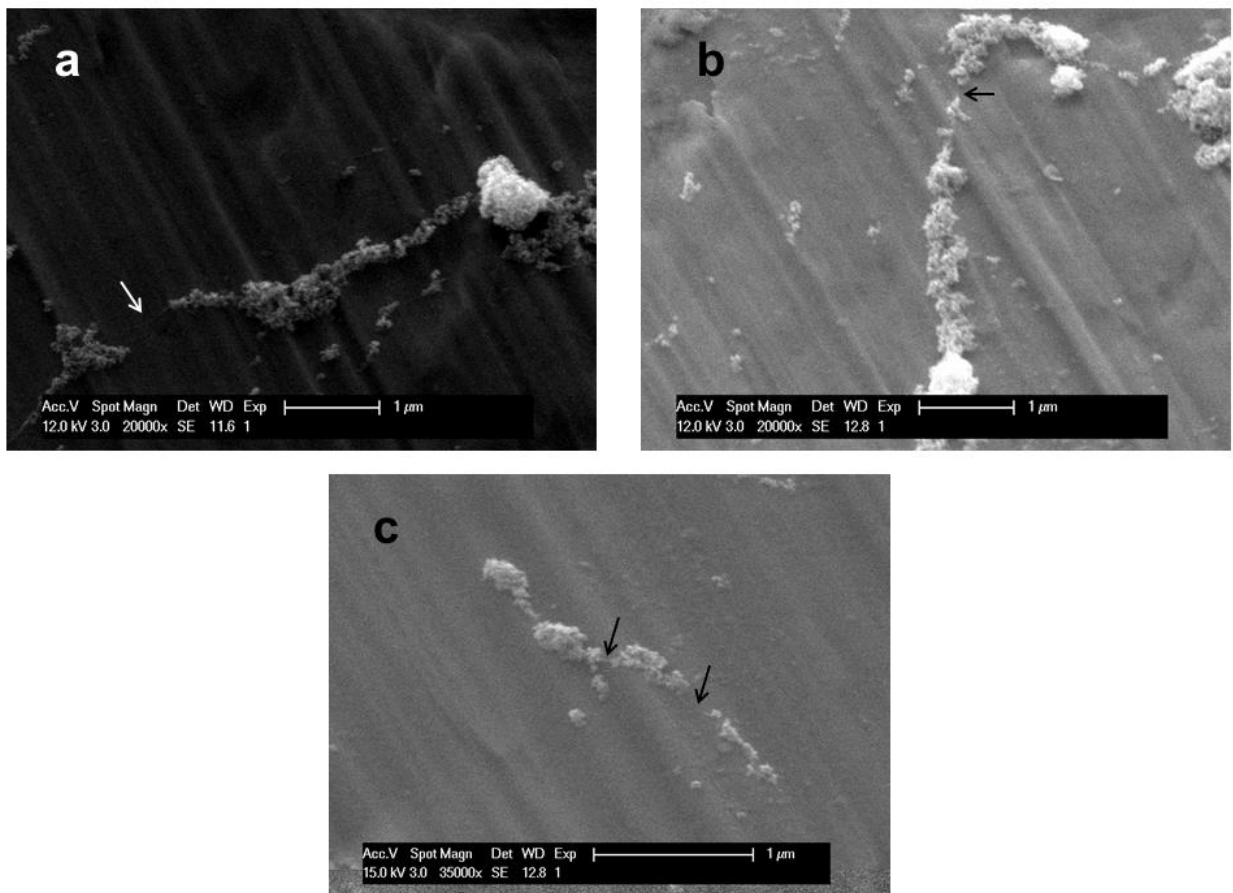


Figure S1. SEM images of $\text{In}_2\text{O}_3/\text{SWCNT}$. (a-c) $\text{In}_2\text{O}_3/\text{SWCNT}$ composite calcinated at 400 $^\circ\text{C}$. All images were prepared on copper tape. Arrows indicate region of bare CNTs, thus showing that the majority of the CNT is surrounded by an In_2O_3 nanoparticle shell.

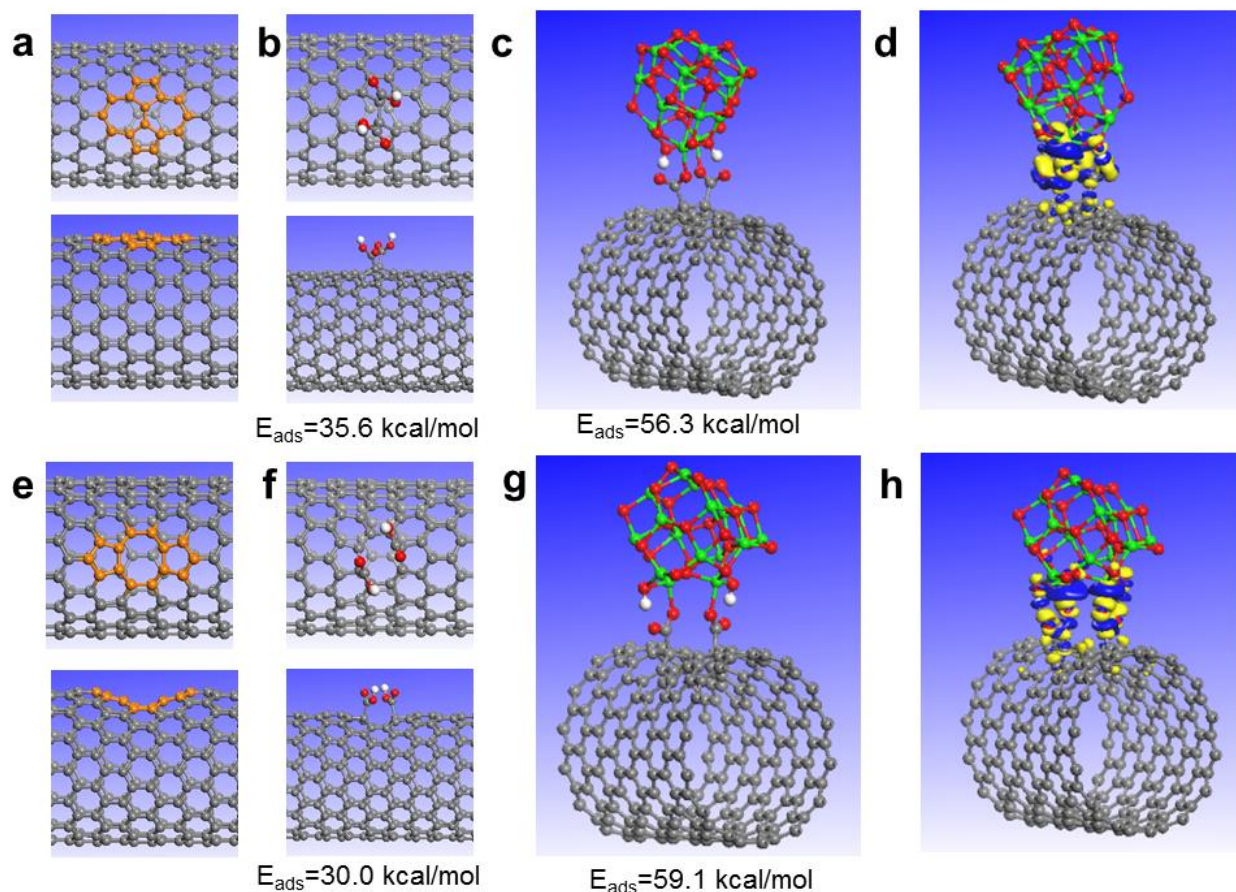


Figure S2. (a),(e) Top and side views of a SWCNT with a Stone-Wales and octagon pentagon pair defect, respectively. For each case the corresponding adsorption configurations of two carboxyl groups adsorbed at the respective topological defects are illustrated in panels (c) for Stone-Wales and (d) octagon pentagon defects. The adsorption energies of the carboxyl group is indicated at the bottom of panels c) and d), respectively. Panels c) and g) illustrate the adsorption of a $(\text{In}_2\text{O}_3)_8$ cluster on the SWCNT with different topological defects functionalized with carboxyl groups. In each case the adsorption energy is indicated at the bottom of respective panels. The corresponding charge difference maps for adsorption of the $(\text{In}_2\text{O}_3)_8$ cluster on carboxyl functionalized SWCNT. In these panels the charge difference was calculated with respect to the OCO-decorated SWCNT and H-decorated oxide, i.e. $\Delta\rho(\mathbf{r})=\rho_{\text{total}}(\mathbf{r})-\rho_{[\text{SWCNT+OCO}]}(\mathbf{r})-\rho_{[\text{oxide+H}]}(\mathbf{r})$.

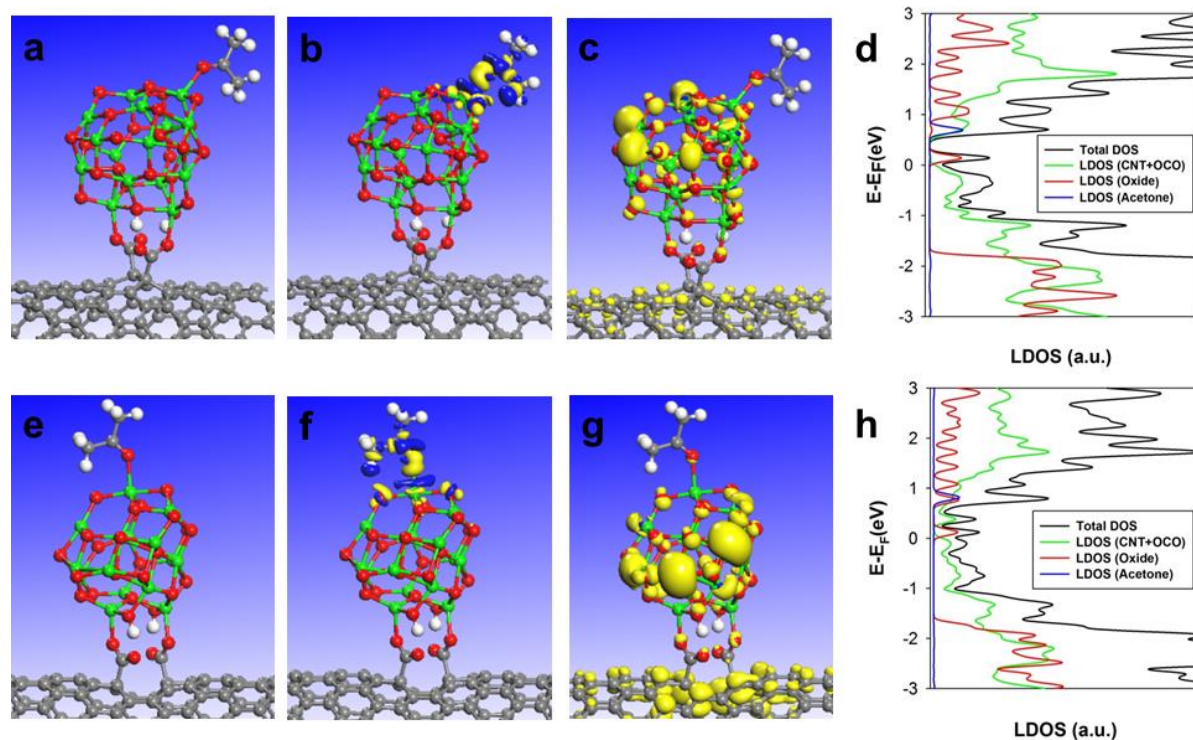


Figure S3. Representative adsorption configurations of acetone on a hybrid $(\text{In}_2\text{O}_3)_8$ cluster-carboxyl-SWCNT with various defects. Top panels (a-d) illustrate the results for SWCNT with a Stone-Wales defect while bottom panels (e-g) present the case of SWCNT with an octagon-pentagon pair defect. In both instances the carboxyl groups initially bonded on the SWCNT at the corresponding topological defects allow formation of new bonds with the In atoms of the oxide cluster while concomitantly the H atoms of the carboxyl are transferred to the oxide cluster. C atoms are grey, In atoms are green, O atoms are red and H atoms are white. In both instances the carboxyl groups are bonded at the corresponding defects. Panels b) and f) represent the charge difference maps for acetone adsorbed on the respective hybrid oxide-carboxyl-SWCNT systems. The indicated isosurfaces correspond to values of $0.015 \text{ e}^-/\text{\AA}^3$ (yellow) and $-0.015 \text{ e}^-/\text{\AA}^3$ (blue). Panels c) and g) illustrate the partial charge density corresponding to the electronic bands situated at and immediately above the top of the valence band. The isosurface of $0.010 \text{ e}^-/\text{\AA}^3$ is shown in both these two cases. In panels d) and h) the total density of states and its projections on the individual SWCNT, oxide and acetone atoms are shown. For increased clarity the contribution of OCO atoms of the carboxyl is included in the LDOS of SWCNT while the contribution of the H atoms residing on the oxide cluster was included in the LDOS of the oxide.

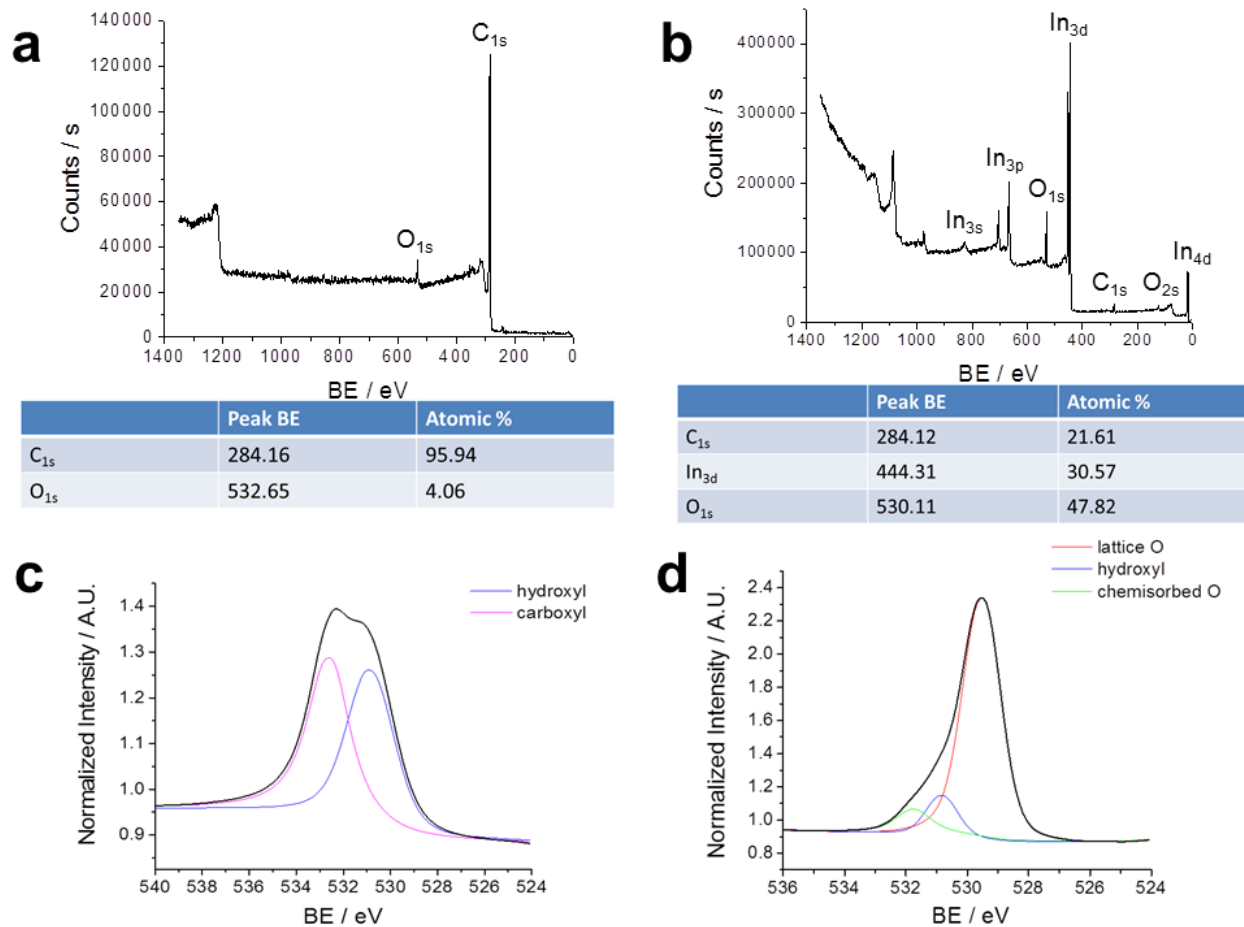


Figure S4. XPS study of oxidized SWCNTs and In₂O₃/SWCNT composite. (a) Survey scan of oxidized SWCNTs, (b) survey scan of In₂O₃/SWCNT composite, (c) high-resolution scan of O_{1s} peak for oxidized SWCNTs, and (d) high-resolution scan of O_{1s} peak for In₂O₃/SWCNT.

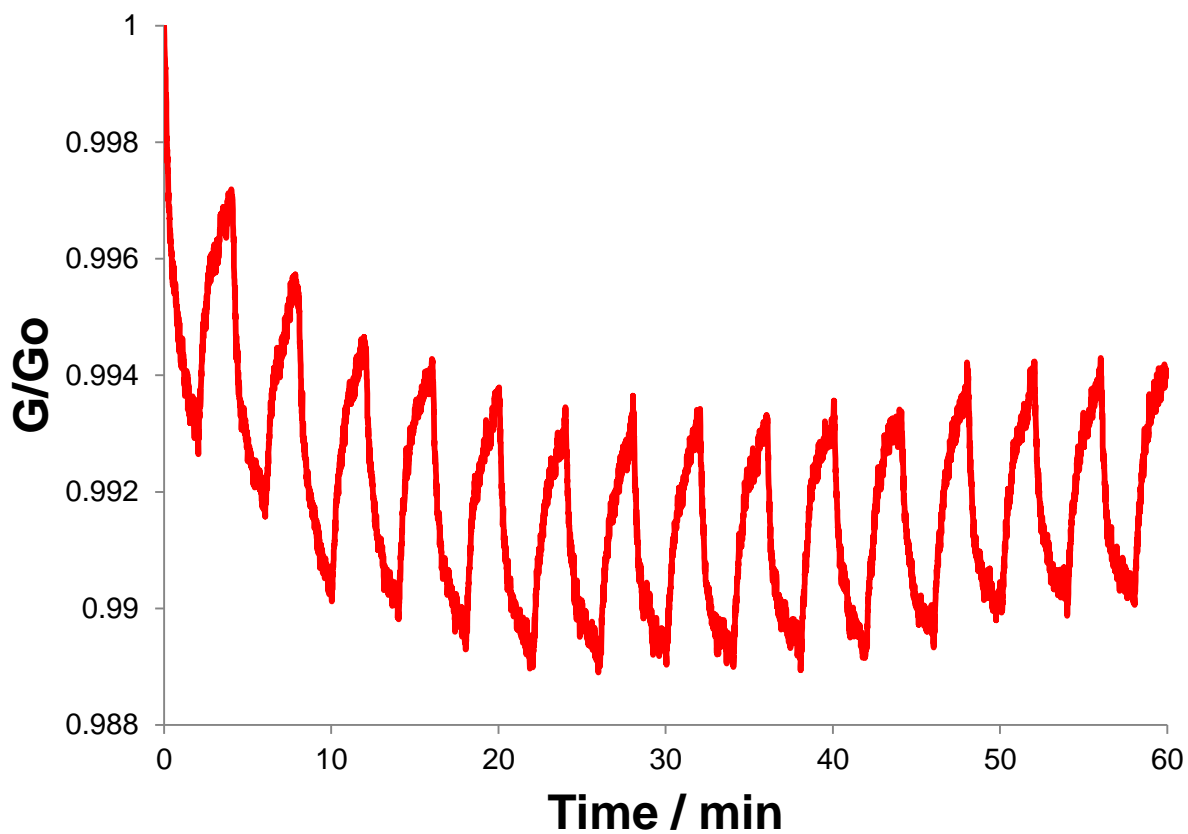


Figure S5. Relative conductance of a sensor exposed to repeated bursts of 10 ppm acetone in dry N₂ over one hour.

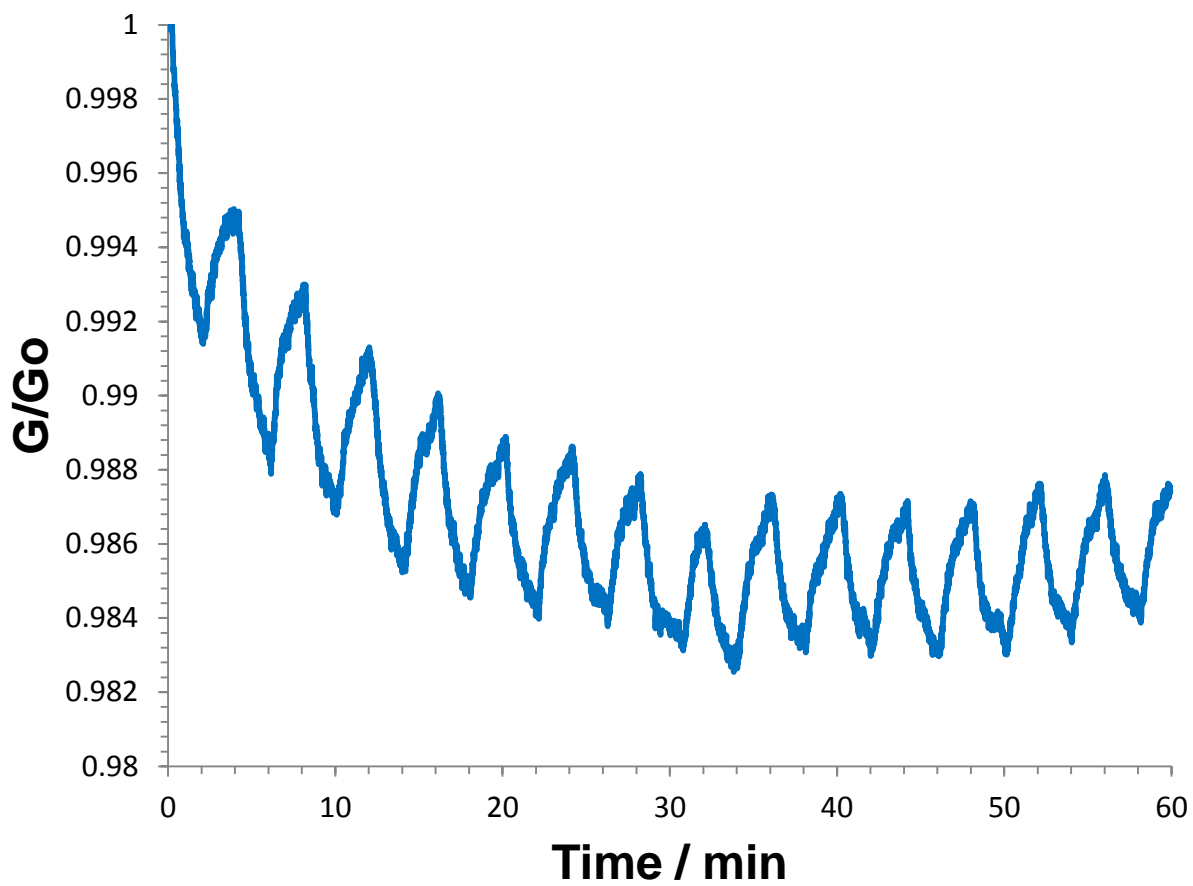


Figure S6. Relative conductance of a sensor exposed to repeated bursts of 10 ppm ethanol in dry N₂ over one hour.

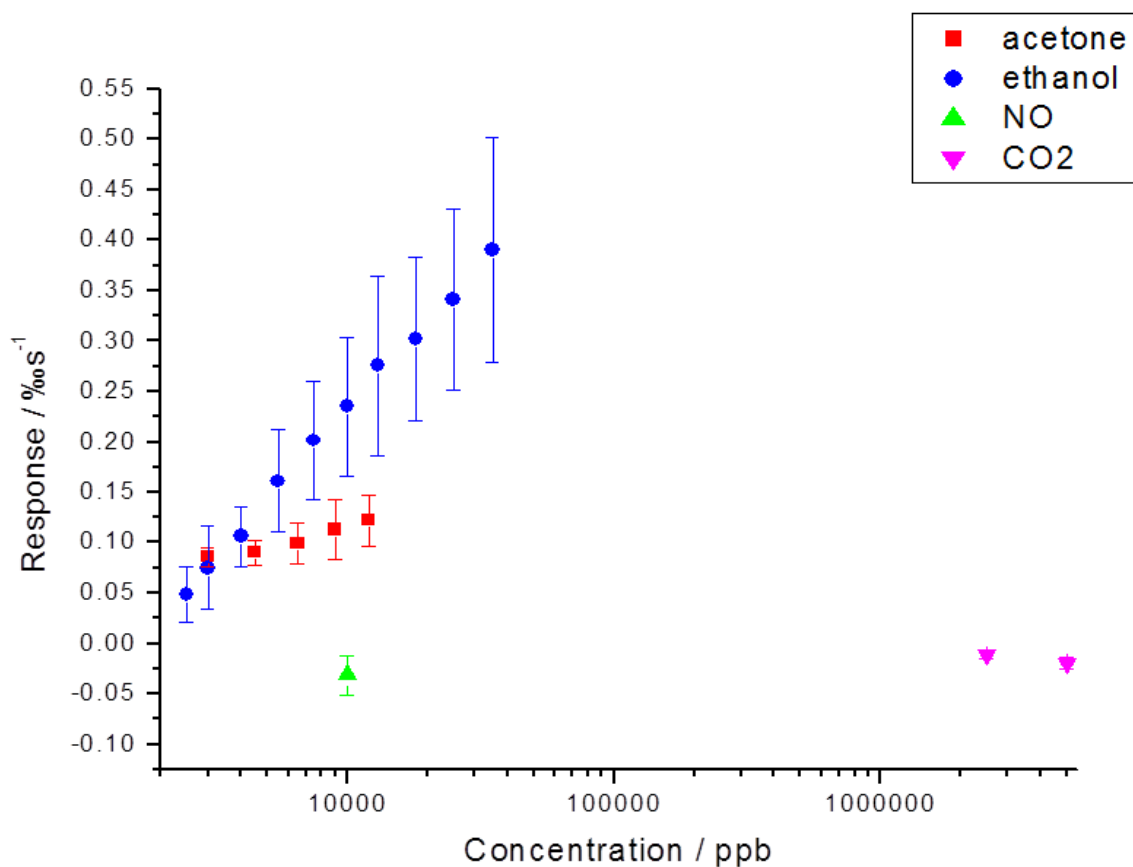


Figure S7. Selectivity of In₂O₃/SWCNT to different gases. In₂O₃/SWCNT sensor was exposed to 300 sccm flows of acetone, ethanol, nitric oxide, and carbon dioxide. Acetone (2, 3, 4.5, 6.5, and 9 ppm) and ethanol (2.5, 3, 4, 5.5, 7.5, 10, 13, 18, 25, 35 ppm) decreased the sensor conductance and had a linear response in the first minute of exposure. Nitric oxide (10 ppm) increased the sensor conductance in the first minute, but there was little to no recovery to the baseline. CO₂ (2500, 5000 ppm) slightly increased the sensor conductance in the first minute at high concentrations.

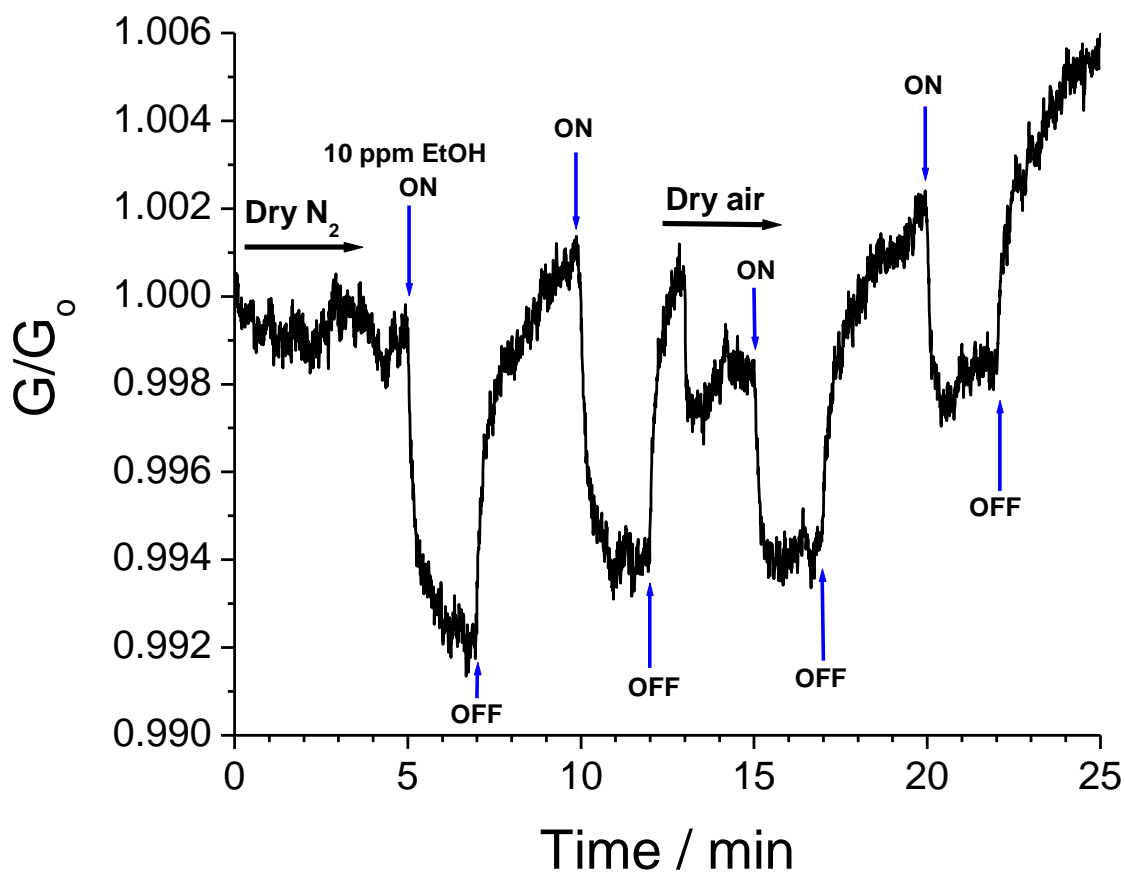


Figure S8. Ethanol sensing in dry air. Dry N₂ (300 sccm) is used as a carrier gas for the initial thirteen minutes. Two 2-minute bursts of 10 ppm ethanol are flowed over the chip using dry N₂ as the carrier gas (5m—7m; 10m—12m). At minute thirteen, the carrier gas is switched to dry air (300 sccm). Two 2-minute bursts of 10 ppm ethanol are flowed over the chip using dry air as the carrier gas (15m—17m; 20m—22m).

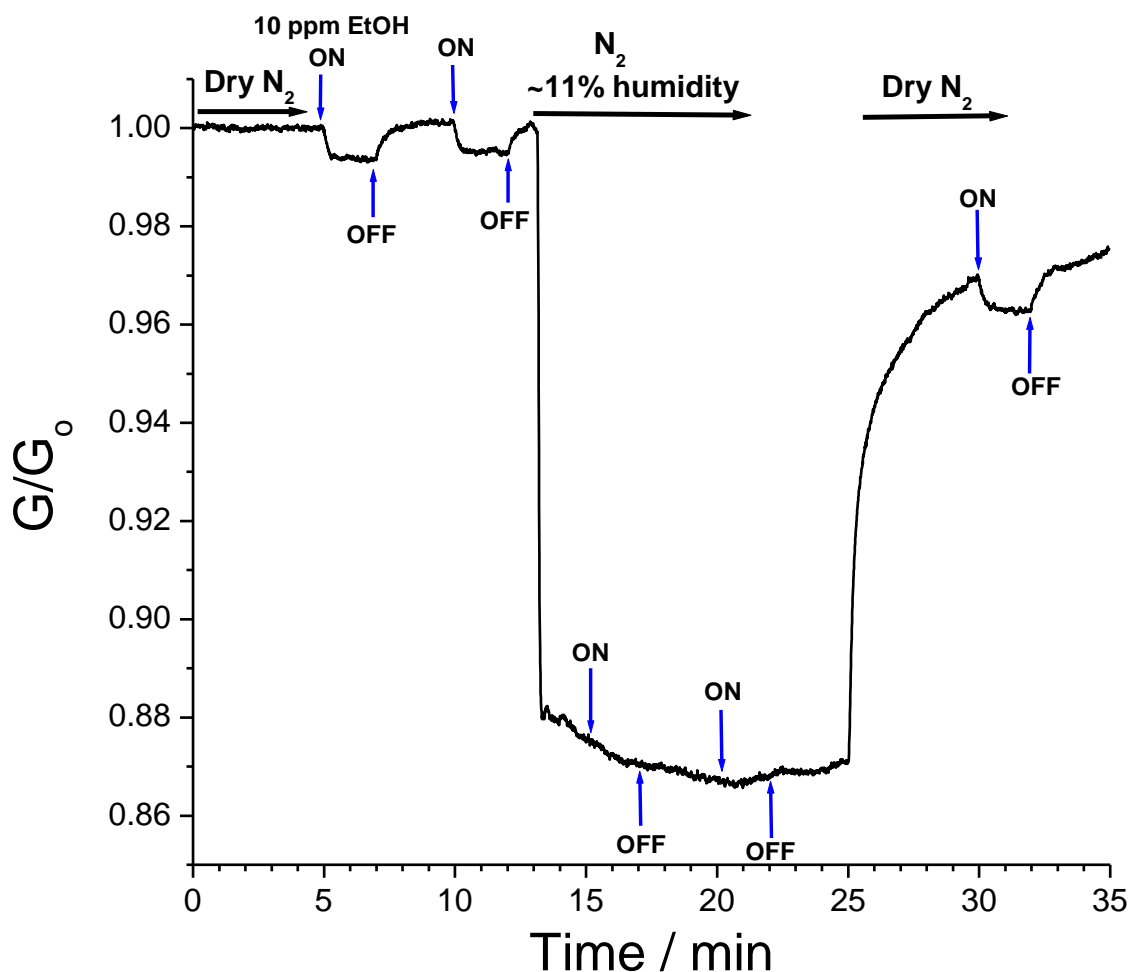


Figure S9. Ethanol sensing in humidity. Dry N₂ (300 sccm) is used as a carrier gas for the initial thirteen minutes. Two 2-minute bursts of 10 ppm ethanol are flowed over the chip using dry N₂ as the carrier gas (5m—7m; 10m—12m). At minute thirteen, the dry N₂ carrier gas is bubbled through a saturated lithium chloride aqueous solution, bringing the humidity of the carrier gas to ~11%.^{S14} Two 2-minute bursts of 10 ppm ethanol are flowed over the chip using ~11% humidity N₂ as the carrier gas (15m—17m; 20m—22m). At minute twenty-five, the carrier gas is switched back to dry N₂. A final 2-minute burst of 10 ppm ethanol is flowed over the chip using dry N₂ as the carrier gas (30m—32m).

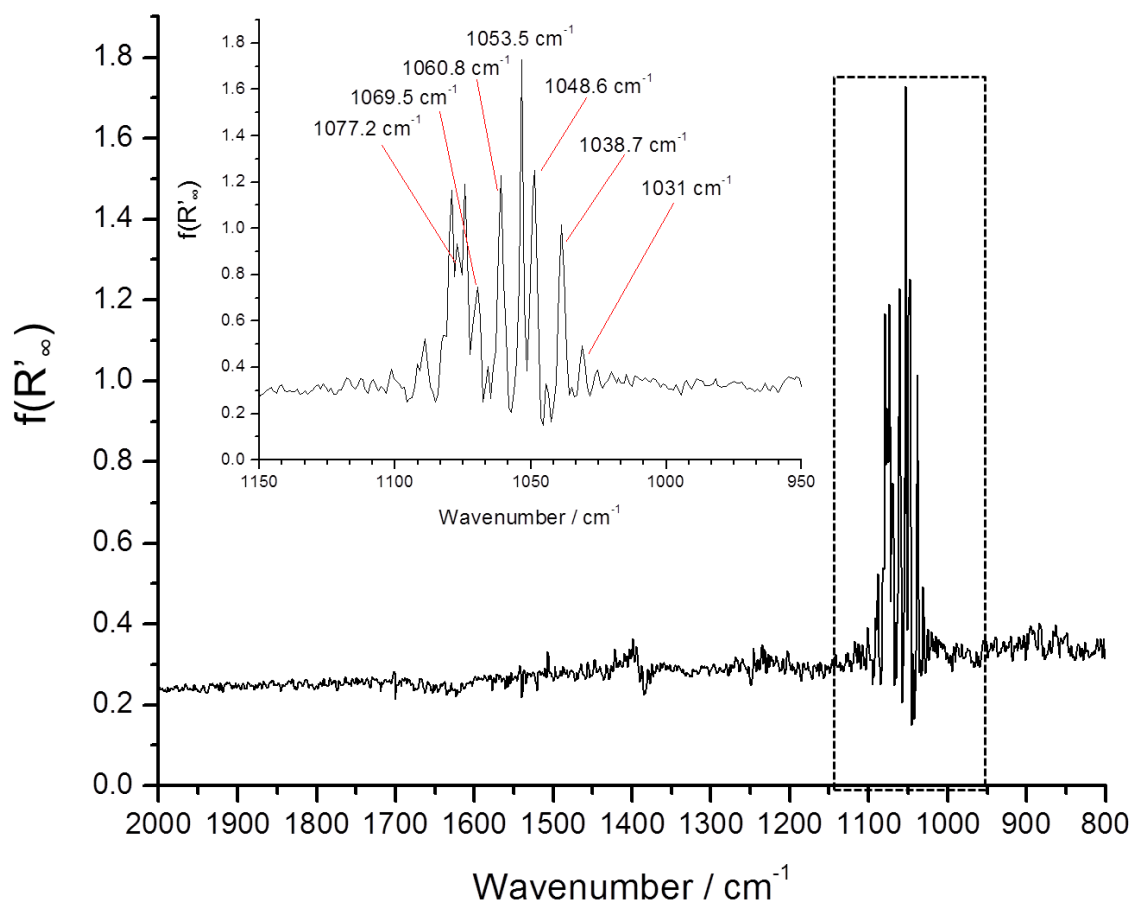
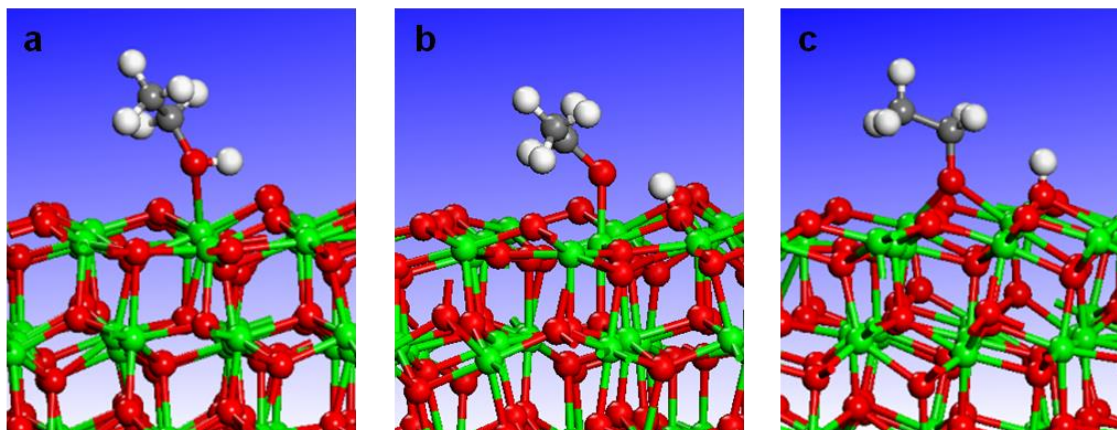


Figure S10. DRIFTS of $\text{In}_2\text{O}_3/\text{SWCNT}$ in the presence of ethanol vapors. $\text{In}_2\text{O}_3/\text{SWCNT}$ composite was calcinated at 400 °C for 0 minutes. The plot is $f(R'_{\infty})$ versus wavenumber, where the function is the Kubelka-Munk equation and R'_{∞} is the ratio of the reflected intensity of the sample to that of KBr. Background Scan: Calcinated $\text{In}_2\text{O}_3/\text{SWCNT}$ mixed with KBr powder. Sample Scan: Calcinated $\text{In}_2\text{O}_3/\text{SWCNT}$ mixed with KBr powder in the presence of ethanol vapors.

Table S1. Comparison of the calculated vibrational frequencies of ethanol (insert panel a) at the bottom of this table) and of the ethoxy species (panels b) and c)) adsorbed on In₂O₃(111) surface. For ethanol the corresponding results for the isolated ethanol molecule in gas phase are also indicated. For ethoxy specie results for the monodentate (m) and bidentate (b) bonding configurations on In₂O₃(111) are indicated. The $\nu(\text{CO})$ vibration changes from 1026 cm⁻¹ for ethanol to 1098 cm⁻¹ for ethoxy (m) and 1048 cm⁻¹ for ethoxy (b). No scaling of calculated vibrations has been considered.

Mode	Ethanol (gas)	Gas Phase Assignment	Ethanol@ In ₂ O ₃ (111)	Ethoxy(m)@ In ₂ O ₃ (111)	Ethoxy(b)@ In ₂ O ₃ (111)
1	3743	$\nu(\text{OH})$	3056	3072	3731
2	3058	$\nu_a(\text{CH}_3)$	3053	3040	3037
3	3058	$\nu_a(\text{CH}_3)$	3050	3014	3029
4	2981	$\nu_a(\text{CH}_3)$	3012	2947	2958
5	2942	$\nu_a(\text{CH}_2)$	2976	2935	2039
6	2915	$\nu_s(\text{CH}_2)$	2972	2869	2913
7	1471	$\delta(\text{CH}_2)$	1464	1455	1461
8	1449	$\delta(\text{CH}_3)$	1443	1434	1439
9	1432	$\delta(\text{CH}_3)$	1438	1428	1436
10	1396	$w(\text{CH}_3) + w(\text{CH}_2)$	1367	1347	1360
11	1349	$\delta_s(\text{CH}_3)$	1363	1335	1342
12	1253	$t_w(\text{CH}_2)$	1347	1269	1266
13	1228	$\delta(\text{OH}) + r(\text{CH}_2)$	1258	1132	1131
14	1134	$t_w(\text{CH}_2) + t_w(\text{CH}_3)$	1108	1098 ($\nu(\text{CO})$)	1081
15	1074	$\nu(\text{CO}) + r(\text{CH}_2)$	1077	1067	1048 ($\nu(\text{CO})$)
16	1010	$\delta(\text{OH}) + r(\text{CH}_3)$	1026 ($\nu(\text{CO})$)	1050	877
17	876	$\delta(\text{CCH})$	874	883	786
18	794	$r(\text{CH}_2) + r(\text{CH}_3)$	831	849	692
19	404	$\delta(\text{CCO})$	784	776	639
20	275	$t_w(\text{COH}) + t_w(\text{CH}_3)$	446	458	483
21	227	$t_w(\text{CH}_3) + t_w(\text{CH}_2) + t_w(\text{COH})$	265	436	354



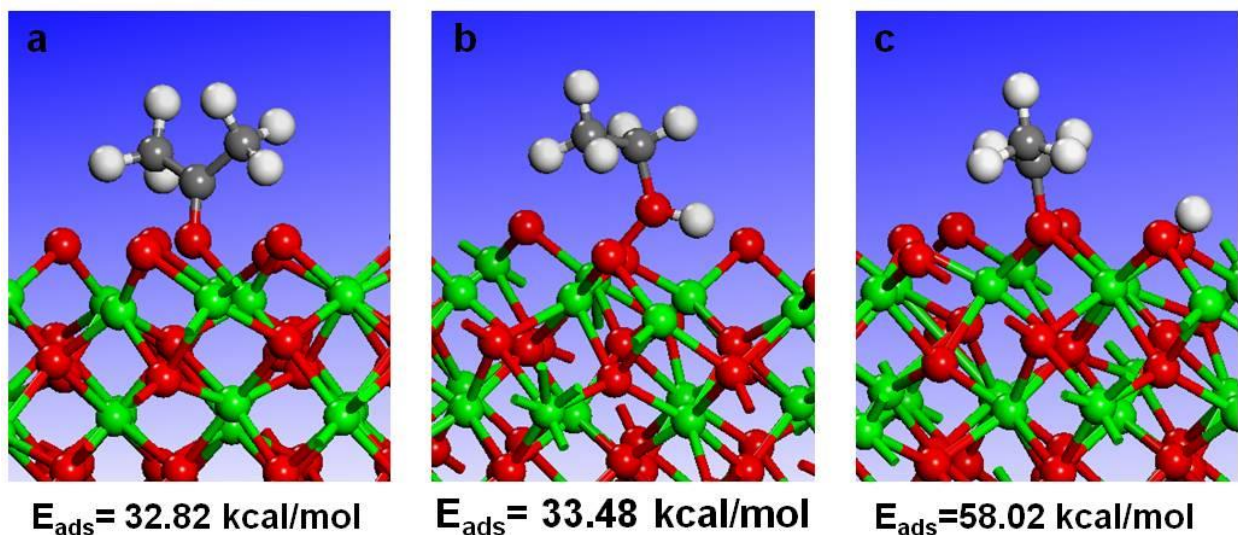


Figure S11. Adsorption of acetone and ethanol to In_2O_3 (001) surface. For this polar surface the model of half-filled oxygen planes developed in Ref. S7 has been considered. Representative adsorption configurations of acetone (a) and ethanol (b,c) adsorbed on In_2O_3 (001) surface. In panel (b) the adsorption of ethanol in a molecular undissociated state is illustrated while panel (c) shows the case when the H atom of ethanol is transferred to the surface with formation of an ethoxy species. The reference of the indicated adsorption energies is taken as the sum of the energies of the isolated surface and isolated adsorbate.

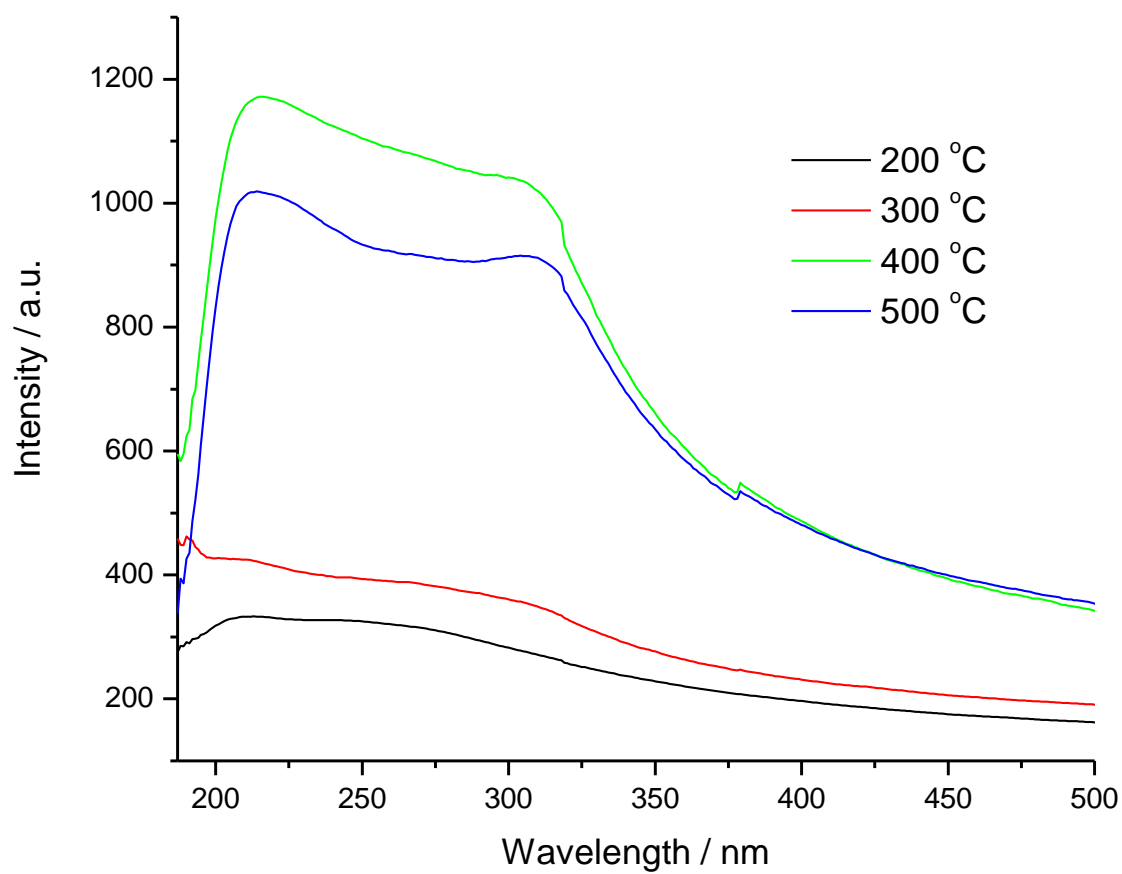


Figure S12. UV-vis absorption spectra of four materials prepared at various calcination temperatures.

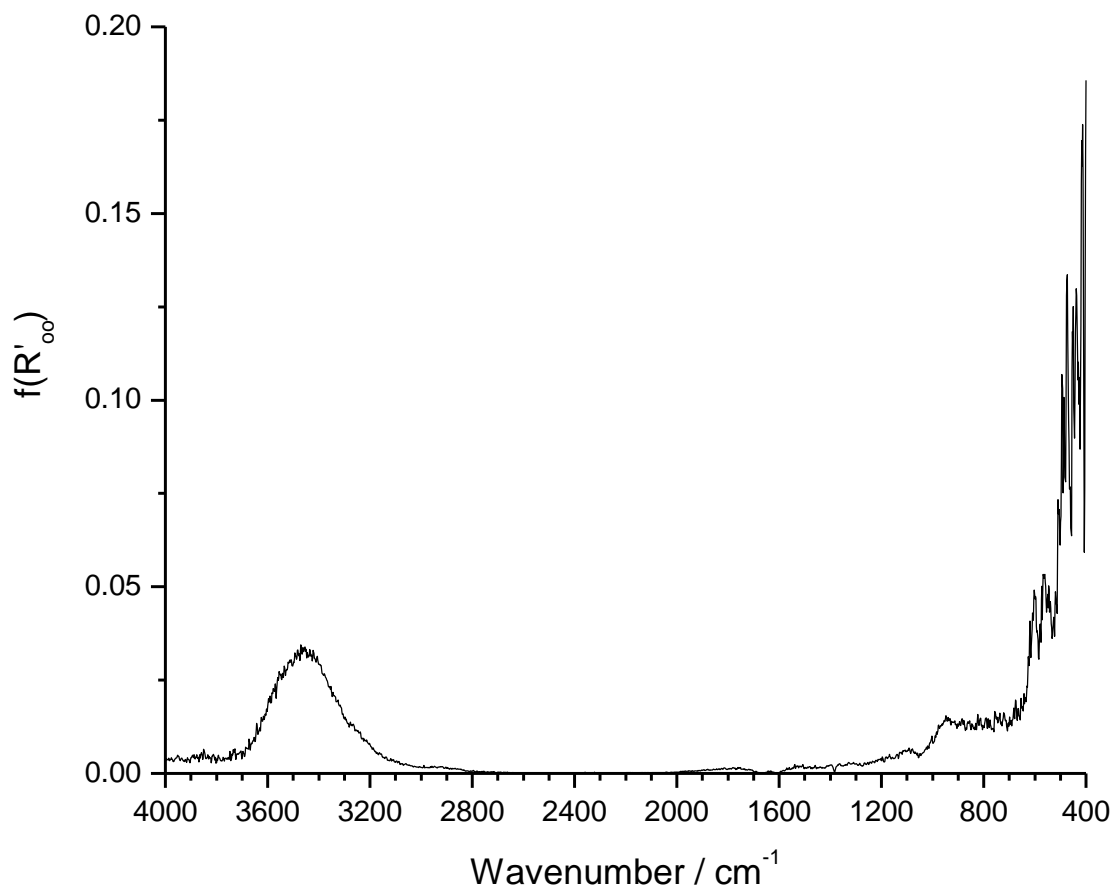


Figure S13. DRIFTS of $\text{In}_2\text{O}_3/\text{SWCNT}$. $\text{In}_2\text{O}_3/\text{SWCNT}$ composite was calcinated at 400 °C for 0 minutes. The plot is $f(R'_{\infty})$ versus wavenumber, where the function is the Kubelka-Munk equation and R'_{∞} is the ratio of the reflected intensity of the sample to that of KBr. Background Scan: KBr powder. Sample Scan: Calcinated $\text{In}_2\text{O}_3/\text{SWCNT}$ mixed with KBr powder.

Supporting Information References

- (S1) Liu, G., Synthesis, Characterization of In₂O₃ Nanocrystals and Their Photoluminescence Property. *Int. J. Electrochem. Sci.* **2011**, *6*, 2162-2170.
- (S2) Kresse, G.; Furthmüller, J., Efficiency of Ab-Initio Total Energy Calculations for Metals and Semiconductors Using a Plane-Wave Basis Set. *Comput. Mater. Sci.* **1996**, *6*, 15-50.
- (S3) Kresse, G.; Furthmüller, J., Efficient Iterative Schemes for Ab Initio Total-Energy Calculations Using a Plane-Wave Basis Set. *Phys. Rev. B* **1996**, *54*, 11169-11186.
- (S4) Perdew, J. P.; Burke, K.; Ernzerhof, M., Generalized Gradient Approximation Made Simple. *Phys. Rev. Lett.* **1996**, *77*, 3865-3868.
- (S5) Blöchl, P. E., Projector Augmented-Wave Method. *Phys. Rev. B* **1994**, *50*, 17953-17979.
- (S6) Kresse, G.; Joubert, D., From Ultrasoft Pseudopotentials to the Projector Augmented-Wave Method. *Phys. Rev. B* **1999**, *59*, 1758-1775.
- (S7) Agoston, P.; Albe, K., Ab Initio Modeling of Diffusion in Indium Oxide. *Phys. Rev. B* **2010**, *81*, 195205.
- (S8) Agoston, P.; Erhart, P.; Klein, A.; Albe, K., Geometry, Electronic Structure and Thermodynamic Stability of Intrinsic Point Defects in Indium Oxide. *J. Phys.: Condens. Matter* **2009**, *21*, 455801.
- (S9) Erhart, P.; Klein, A.; Egdell, R. G.; Albe, K., Band Structure of Indium Oxide: Indirect Versus Direct Band Gap. *Phys. Rev. B* **2007**, *75*, 153205.
- (S10) Monkhorst, H. J.; Pack, J. D., Special Points for Brillouin-Zone Integrations. *Phys. Rev. B* **1976**, *13*, 5188-5192.
- (S11) Walsh, A.; Woodley, S. M., Evolutionary Structure Prediction and Electronic Properties of Indium Oxide Nanoclusters. *Phys. Chem. Chem. Phys.* **2010**, *12*, 8446-8453.
- (S12) Bader, R. F. W., *Atoms in Molecules: A Quantum Theory*. Oxford University Press: New York, 1994.
- (S13) Sanville, E.; Kenny, S. D.; Smith, R.; Henkelman, G., Improved Grid-Based Algorithm for Bader Charge Allocation. *J. Comput. Chem.* **2007**, *28*, 899-908.
- (S14) Greenspan, L., Humidity Fixed Points of Binary Saturated Aqueous Solutions. *J. Res. Nat. Bur. Stand. Sect. A* **1977**, *81A*, 89-96.